Geochemistry, Geophysics, Geosystems®

AGU ADVANCING EARTH AND SPACE SCIENCE

RESEARCH ARTICLE
10.1029/2021GC010214

Multitechnique Geochronology of Intrusive and Explosive Activity on Piton des Neiges Volcano, Réunion Island

Vincent Famin[1,2], Camille Paquez[1,2,3], Martin Danišík[4], Nicholas J. Gardiner[5,6], Laurent Michon[1,2], Christopher L. Kirkland[6], Carole Berthod[7], Bjarne Friedrichs[8,9], Axel K. Schmitt[8], and Patrick Monié[10]

[1]Institut de physique du globe de Paris, Université Paris Cité, CNRS, Paris, France, [2]Laboratoire GéoSciences Réunion, Université de La Réunion, Saint-Denis, France, [3]Austral Energy, Saint-Pierre, France, [4]John de Laeter Centre, Curtin University, Perth, WA, Australia, [5]Now at School of Earth and Environmental Sciences, University of St. Andrews, St. Andrews, United Kingdom, [6]School of Earth and Planetary Sciences, Timescales of Mineral Systems Group, Curtin University, Perth, WA, Australia, [7]Laboratoire Magmas et Volcans, Université Clermont-Auvergne, CNRS, IRD, OPGC, Aubière, France, [8]Institute of Earth Sciences, Ruprecht-Karls-Universität Heidelberg, Heidelberg, Germany, [9]Department of Environment & Biodiversity, Paris-Lodron-Universität Salzburg, Salzburg, Austria, [10]Géosciences Montpellier, Université de Montpellier, CNRS, Université des Antilles, Montpellier, France

Abstract The construction of ocean island basaltic volcanoes consists of a succession of eruptions, intrusions, and metamorphism. These events are often temporally ill-constrained because the most widely used radiometric dating methods applicable to mafic volcanic rocks (K-Ar or $^{40}Ar/^{39}Ar$ on whole rock or groundmass) are prone to inaccuracy when applied to slowly cooled, altered, or vesicular and aphyric products. Here, we adopt a multitechnique geochronology approach (including zircon U-Pb, phlogopite $^{40}Ar/^{39}Ar$, zircon and apatite (U-Th)/He, and zircon double-dating) to demonstrate its efficacy when applied to basaltic volcanoes. Taking the main volcano of Réunion Island (Piton des Neiges) as a case study, we establish the time of the major plutonic, metamorphic, and explosive events that had resisted previous dating attempts. We document four stages of pluton emplacement and metamorphism at 2,200–2,000 ka, 1,414 ± 8 ka, 665 ± 78 ka, and 150–110 ka, all coinciding with volcanism revival after quiescent intervals. We also date a major Plinian eruption at 188.2 ± 10.4 ka, coeval with the formation age of a large caldera, and, finally, we constrain the last eruption of Piton des Neiges to 27 ka, revising a previous estimate of 12 ka. By resolving several conundrums of Réunion's geological history, our multitechnique geochronology approach reveals that endogenous growth of a volcanic island proceeds as pulses at the beginning of renewed volcanism. We also demonstrate that crosschecking eruptions ages by diversified dating techniques is important to better assess the timing and recurrence of basaltic volcanic activity, with implications for hazard prediction.

Plain Language Summary Dating techniques based on natural radioactivity span multiple isotopes and minerals. However, geochronology of volcanic islands remains challenging due to the extremely low radioactivity of erupted products—mostly basalts (including their mineral cargo). Consequently, many events in the geological history of these islands, like explosive eruptions or magma intrusions, remain challenging to date. To resolve this issue, we test the efficacy of six dating methods, unusually applied to a basaltic volcanic island and never in combination. Taking Piton des Neiges volcano (Réunion Island) as a natural laboratory, we demonstrate that combining these techniques is not only feasible, but also productive in terms of the recovered geological information. We obtain ages for many rocks of Réunion that resisted other techniques, or whose age has previously remained controversial. In particular, we date a major explosion at 188,000 years, and constrain the last eruptive activity of Piton des Neiges to 27,000 years, revising a previous estimate of 12,000 years. The new ages also show that significant volumes of magma must have remained stored inside the edifice at the beginning of active periods. Our combined approach thus offers a promising solution to reconstruct the history of volcanic islands and better predict their hazard.

Key Points:

- First application of zircon-phlogopite-apatite geochronology to a hotspot island
- Endogenous growth proceeds as pulses at the beginning of renewed volcanism
- Last volcanism of Piton des Neiges is 27 ka, not 12 ka as earlier proposed

Supporting Information:

Supporting Information may be found in the online version of this article.

Correspondence to:

V. Famin,
vfamin@univ-reunion.fr

Citation:

Famin, V., Paquez, C., Danišík, M., Gardiner, N. J., Michon, L., Kirkland, C. L., et al. (2022). Multitechnique geochronology of intrusive and explosive activity on Piton des Neiges volcano, Réunion Island. *Geochemistry, Geophysics, Geosystems*, *23*, e2021GC010214. https://doi.org/10.1029/2021GC010214

Received 14 OCT 2021
Accepted 28 FEB 2022

Author Contributions:

Conceptualization: Vincent Famin, Laurent Michon
Data curation: Vincent Famin, Carole Berthod
Formal analysis: Martin Danišík, Nicholas J. Gardiner, Christopher L. Kirkland
Funding acquisition: Vincent Famin, Martin Danišík
Investigation: Vincent Famin, Camille Paquez, Martin Danišík, Nicholas J. Gardiner, Laurent Michon, Carole Berthod

1. Introduction

Geochronological constraints on ocean basaltic volcanoes are essential for the understanding of many aspects in the geodynamics of hotspots and mantle plumes. Radiometric ages, for instance, have proved critical in the identification of temporal geochemical variations in magmas, which informs about the composition and structure

Methodology: Martin Danišík, Nicholas J. Gardiner, Christopher L. Kirkland, Bjarne Friedrichs, Axel K. Schmitt, Patrick Monié
Project Administration: Vincent Famin
Resources: Vincent Famin, Camille Paquez, Carole Berthod
Software: Martin Danišík, Nicholas J. Gardiner, Bjarne Friedrichs, Axel K. Schmitt, Patrick Monié
Supervision: Vincent Famin
Validation: Martin Danišík, Nicholas J. Gardiner, Christopher L. Kirkland, Bjarne Friedrichs, Axel K. Schmitt, Patrick Monié
Visualization: Vincent Famin
Writing – original draft: Vincent Famin
Writing – review & editing: Vincent Famin, Camille Paquez, Martin Danišík, Nicholas J. Gardiner, Laurent Michon, Christopher L. Kirkland, Carole Berthod, Bjarne Friedrichs, Axel K. Schmitt, Patrick Monié

of mantle plumes (e.g., Kurz et al., 1987). Geochronology is also of prime importance for reconstructing the geological history of volcanic islands, and thus for identifying periods of both activity and quiescence of hotspot volcanism (e.g., Guillou et al., 1996). For these and many other reasons, since the early 1970s a huge amount of work has been devoted to the K-Ar and $^{40}Ar/^{39}Ar$ dating of ocean island volcanic products, primarily because these techniques are applicable to young (≤2 Ma) mafic rocks such as basalts.

However, the widespread use of K-Ar and $^{40}Ar/^{39}Ar$ dating on whole rock or groundmass may introduce a potential bias in our understanding of how basaltic volcanic islands evolve, because of some limitations inherent in these techniques (e.g., accuracy dependent on K concentration, open-system behavior of K or Ar, mass-dependent kinetic isotopic fractionation of Ar in glasses, presence of undetected xenocrysts) (McDougall & Harrison, 1999; Morgan et al., 2009; Quidelleur et al., 1999; Spell et al., 2001). In practice, these limitations lead workers to prioritize dating on: (a) quickly cooled rocks such as lavas or small intrusions in order to prevent radiogenic argon loss; (b) massive, nonaltered and nonvesiculated rocks in order to reduce their interaction with atmospheric argon; or (c) volcanic products containing K-rich phases such as sanidine. This leads to an under-representation of slowly cooled intrusions, metamorphosed rocks, or highly vesicular and aphyric explosive deposits in dated rock units, which in turn may bias our assessment of how endogenous magma emplacement contributes to the edification of a volcano, or of the hazard represented by explosive activity.

Réunion (Figure 1) is a basaltic volcanic island where such a dating bias may exist. This island represents the most recent manifestation of the Réunion hotspot that produced a volcanic chain starting with the Deccan traps ~65 Ma ago (e.g., Duncan, 1990). Réunion is one of the best studied volcanic islands with >500 published radiometric ages—mostly K-Ar—over its two volcanoes: Piton de la Fournaise—active, and Piton des Neiges—the main edifice now inactive and eroded (e.g., Salvany et al., 2012; Singer et al., 2014 and references therein). However, those ages mostly concern fresh and massive lavas, whereas plutonic rocks, although well exposed on Piton des Neiges, have resisted K-Ar dating attempts (e.g., McDougall, 1971). As a result, endogenous growth is largely overlooked. Another bias comes from the difficulty in dating highly vesicular explosive and aphyric products corresponding to the terminal volcanism of Piton des Neiges, which have yielded contradictory ages ranging from 29 to 12 ka, a factor of two difference depending on the technique employed (Delibrias et al., 1986; Deniel et al., 1992; Kluska, 1997), with the consequence that the hazard represented by this volcano is poorly estimated.

The objective of this study is to develop geochronological tools for hotspot islands, by using Réunion as a natural laboratory and testing several dating techniques that have seldom been applied to basaltic volcanoes, and never in combination. We apply six radiometric dating techniques (zircon U-Pb, phlogopite $^{40}Ar/^{39}Ar$, zircon (U-Th)/He, apatite (U-Th)/He, and combined U-Th-Pb and (U-Th)/He zircon dating—a.k.a. zircon double-dating or ZDD) to resolve some longstanding controversies about the timing of intrusive, metamorphic and explosive events at Piton des Neiges. These results allow us to draw some inferences about how endogenous growth proceeds in volcanic islands. Our work also provides a framework to better estimate the explosive hazard represented by basaltic volcanoes, based on the crosscomparison of different dating techniques.

2. Geological Setting

The emerged portion of Piton des Neiges has been classified into five eruptive periods separated by lulls, based on field geology, major element geochemistry and K-Ar dating (Figure 1) (see latest review by Salvany et al., 2012). The first three periods LM (2,200–1,800 ka), PN1 (1,400–950 ka), and PN2 (650–430 ka) correspond to the shield building stage of the volcano with a dominant emission of mafic, olivine-rich magmas. In the inner parts of Piton des Neiges, a yet undated lower greenschist to prehnite-pumpellyite metamorphic event affects the LM and PN1 periods but not PN2. Two additional periods subdivide the postshield stage of Piton des Neiges, PN3 (340–180 ka) with the emission of differentiated, often plagioclase-rich magmas, and PN4 (<140 ka) corresponding to mugearitic to trachytic magmas. Several explosive events occurred in PN3 and PN4, mostly during the 210–180 ka interval, which corresponds to the formation of a caldera and the emission of pyroclastic flows, and also during the terminal activity of Piton des Neiges within the last 70 ka.

Piton des Neiges is incised by three "cirques" (subcircular depressions) (Figure 1) that expose the inner structure of the volcano, including a suite of intrusions. The largest intrusion is a pluton, ≥10 km in diameter according to gravimetry and scientific drillings (e.g., Gailler & Lénat, 2012), cropping out in the cirque of Salazie (north of Piton des Neiges summit). This pluton is made of layered peridotites, gabbros and ferrogabbros (Berthod

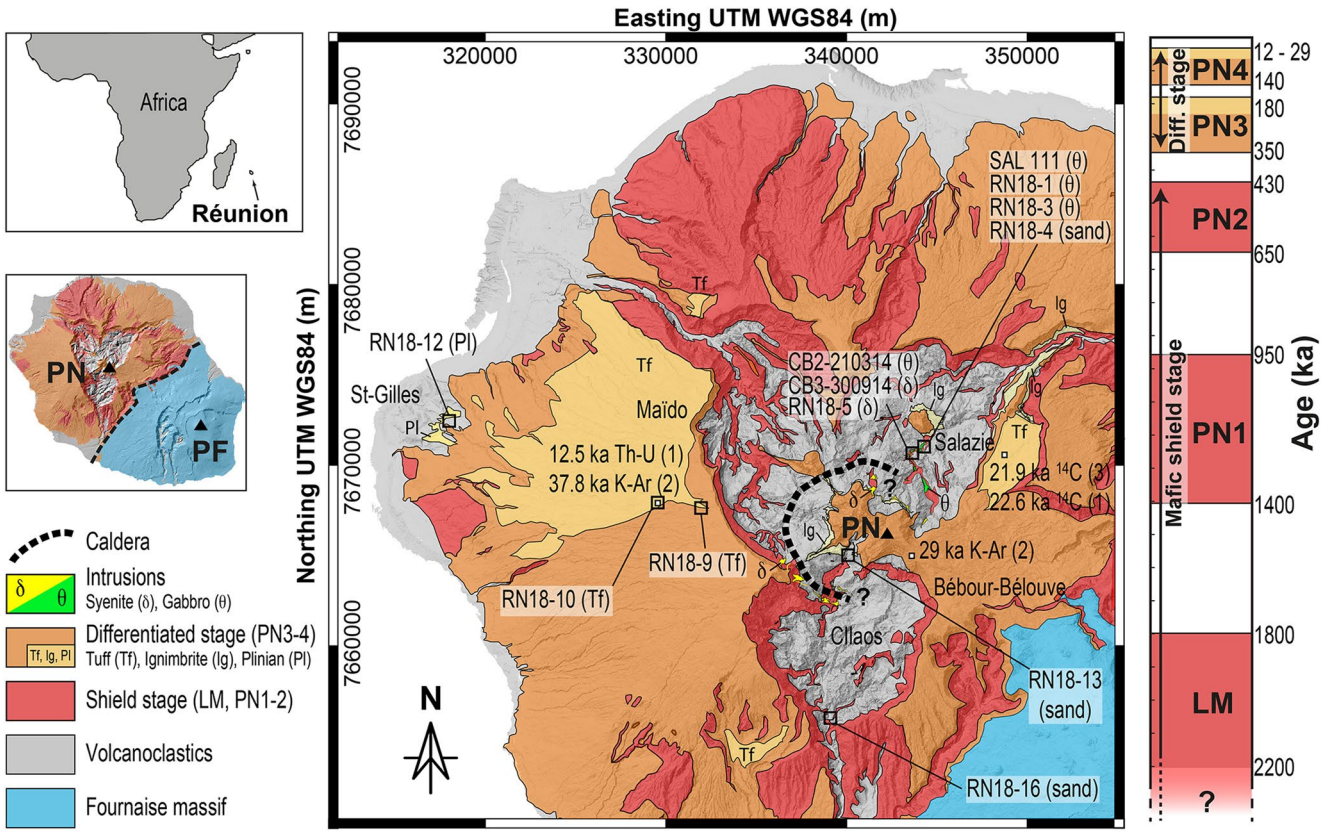

Figure 1. Simplified geology of Piton des Neiges massif (Réunion Island) subdivided by periods of volcanic activity (LM and PN1–PN4) (Salvany et al., 2012). Rocks are lava flows unless specified in the legend. Also added are sample locations and proposed ages of terminal volcanic activity (1: ^{230}Th-^{238}U and ^{14}C ages of Deniel et al., 1992; 2: K-Ar and ^{14}C ages of Kluska, 1997; 3: ^{14}C age of Delibrias et al., 1986). PN, Piton des Neiges; PF, Piton de la Fournaise.

et al., 2020), which could not be dated despite unpublished attempts by K-Ar (Bachèlery, pers. com.). The top of this pluton is sheared and intruded by many sills (Berthod et al., 2016; Chaput et al., 2014; Famin & Michon, 2010), making any observation of the host rock contact impossible. The only chronological criteria available for this pluton is a greenschist to prehnite-pumpellyite metamorphism (150°–240°C) (Famin et al., 2016), implying a cooling age older than the PN2 period (650–430 ka). The pluton is crosscut by a syenite laccolith, undeformed and unaltered (Berthod et al., 2020). The cirque of Cilaos (south of the volcano summit) also exposes a series of ≥30 m-thick syenite dykes, some of which run over several kilometers and crosscut all the shield building units, and possibly also PN3 units. A previous K-Ar dating attempt of a syenite dyke has revealed a contamination by extraneous radiogenic argon, making the ages unreliable (age range between 3.02 ± 0.12 and 35 ± 0.4 Ma) (McDougall, 1971).

The timing of the latest eruption of Piton des Neiges, which is represented by trachytic tephras, is another matter of debate. Pumice fallout from a major Plinian eruption cover up the lower western slopes of Piton des Neiges in the Saint-Gilles area (Figure 1). However, the age of this eruption remains unknown because the pumice is highly vesicular and aphyric, and hence not appropriate for K-Ar or ^{40}Ar/^{39}Ar dating. Another of these deposits on the upper Maïdo slopes has been dated by ^{230}Th-^{238}U disequilibrium on whole rock and magnetic minerals at 12.5 ± 3 ka (Deniel et al., 1992). However, the coordinates of the dated sample correspond to an inaccessible cliff and must thus be erroneous. Second, Kluska (1997) resampled this deposit according to the map and locality description provided by Deniel et al. (1992), and redated it to 37.8 ± 6 ka by K-Ar on groundmass. In absence of a third dating technique, it is therefore impossible to choose which age estimate is accurate. Other trachytic pumice deposits in the Bébour-Bélouve area (Figure 1) contain charcoal giving several ^{14}C ages, the youngest of which is 21.9 ± 0.7 ka (Delibrias et al., 1986). All the ^{14}C ages, however, were published prior to the establishment of calibration curves. The present-day summit area of Piton des Neiges comprises benmoreite lava flows dated at

29 ± 4 ka (K-Ar on groundmass) (Kluska, 1997), which represents a third possible age estimate for the cessation of volcanism.

3. Materials and Methods

3.1. Samples and Mineral Preparation

Twelve samples were collected to fill gaps among the undated geological units of Piton des Neiges (Figure 1). Six samples belong to the intrusive rocks exposed in the cirques, four of which are gabbros collected at two different exposures of the major plutonic complex of Salazie. The first outcrop ("Site 4" in Berthod et al., 2020) is located beneath a suspended bridge over the Mât river (samples RN18-1, RN18-3, and SAL111). The second gabbro outcrop ("Site 3" in Berthod et al., 2020) is located ∼700 m south of Site 4 in the Mât river canyon (sample CB2-210314). The two other intrusive rock samples (RN18-5, CB3-300914) are syenites from the Salazie laccolith also collected in the Mât river at Site 3.

Three samples are trachytic tephras collected on the erosively less incised, and therefore presumably most recent, western slopes of Piton des Neiges, with the objective of dating its last volcanic activity (Figure 1). One sample (RN18-9) was taken on the upper slopes of the Maïdo. Another sample (RN18-10) was collected on a forest road outcrop in the Maïdo area, at the very same place of the K-Ar age (37.8 ± 6 ka) reported by Kluska (1997), and presumably also the ^{230}Th-^{238}U age (12.5 ± 3 ka) of Deniel et al. (1992). The third sample (RN18-12) comes from the Saint-Gilles Plinian deposit, on the lower western slopes of Piton des Neiges.

The remaining three samples are sands collected in the Mât river at Site 4 in the cirque of Salazie (RN18-4), and in the Bras Rouge river upstream (RN18-13) and downstream (RN18-16) in the cirque of Cilaos.

Samples were crushed and zircon, apatite, or phlogopite crystals were separated using standard magnetic and heavy liquids separation procedures. Zircon crystals from intrusive rocks for U-Pb analysis were hand-picked, mounted in epoxy, ground, polished and imaged by cathodoluminescence (CL) using a Mira3 Scanning Electron Microscope (at the John de Laeter Centre–JdLC, Curtin University) to document internal zonation patterns and identify recrystallization textures. Zircon and apatite crystals from intrusive rocks and sands for (U-Th)/He dating were hand-picked following the strict selection criteria with regard to their size, shape and clarity (Farley, 2002), photographed and individually loaded into platinum (apatite) or niobium microtubes (zircon). Zircon crystals from trachytic tephras for zircon double-dating were hand-picked, rinsed in cold HF to remove adherent glass and pressed into indium (In) metal with unpolished crystal faces exposed at the surface for dating by U-Th-disequilibrium or U-Pb methods using secondary ionisation mass spectrometry (SIMS). Phlogopite crystals were hand-picked and ultrasonically cleaned in acetone and distilled water for ^{40}Ar/^{39}Ar dating.

3.2. Dating Methods

The samples were dated using a range of dating procedures that are detailed in Supporting Information S1. In brief, zircon from intrusive rocks was U-Pb dated using laser ablation multicollector inductively coupled plasma mass spectrometry (LA-MC-ICPMS) on a Nu Plasma II Multi Collector Mass Spectrometer at the GeoHistory Facility, JdLC (Curtin University). ^{40}Ar/^{39}Ar analyses of phlogopite were conducted with an Argus VI multicollector mass spectrometer at Géosciences Montpellier geochronology Laboratory (France). Zircon crystals from trachytic tephras were dated using the ZDD approach (Danišík et al., 2017, 2020), which combined U-Th-disequilibrium (or U-Pb) dating via secondary ionization mass spectrometry (SIMS) on the CAMECA IMS 1280-HR at the HIP Laboratory (Heidelberg University, Germany) and (U-Th)/He dating carried out at the Western Australia Thermochronology Hub (WATCH) Facility (JdLC, Curtin University). The ZDD approach was employed in order to determine U-series disequilibrium correction for (U-Th)/He system in zircon (Farley et al., 2002), given that expected eruption ages were in the 29–12 ka range (see Geological Setting). (U-Th)/He dating of zircon and apatite from intrusive rocks and sands was carried out at the WATCH Facility (JdLC, Curtin University) and followed the conventional single grain dating protocols (e.g., Danišík, Štěpančíková, & Evans, 2012; Danišík, Kuhlemann, et al., 2012). This is because these crystals were assumed not to require a correction for disequilibrium (Farley et al., 2002) given their crystallization age of >1.5 Ma determined beforehand by zircon U-Pb geochronology.

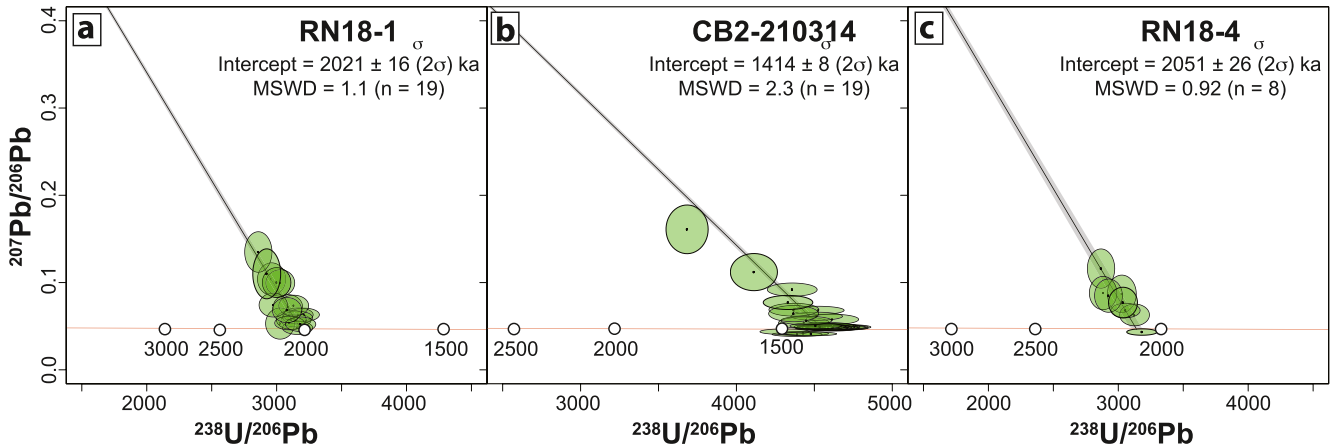

Figure 2. Tera-Wasserburg Concordia diagrams for zircon U-Pb data; error ellipses are 2σ. Ages determined from the intersection on concordia of a projection from the age-corrected common Pb value from Stacey and Kramers (1975). All analyses where $f^{207} > 30\%$ (i.e., large proportion of common Pb) are excluded from age calculations, and not plotted (but are made available in Famin et al., 2022).

4. Results

Zircon U-Pb, phlogopite $^{40}Ar/^{39}Ar$, zircon and apatite (U-Th)/He (hereafter called ZHe and AHe, respectively), and ZDD analyses are available as an EarthChem data set (Famin et al., 2022) and are graphically presented in Figures 2–4. U-Th-disequilibrium and U-Pb SIMS data used for ZDD are also available in EarthChem. A summary of sample locations and dating results is provided in Table 1.

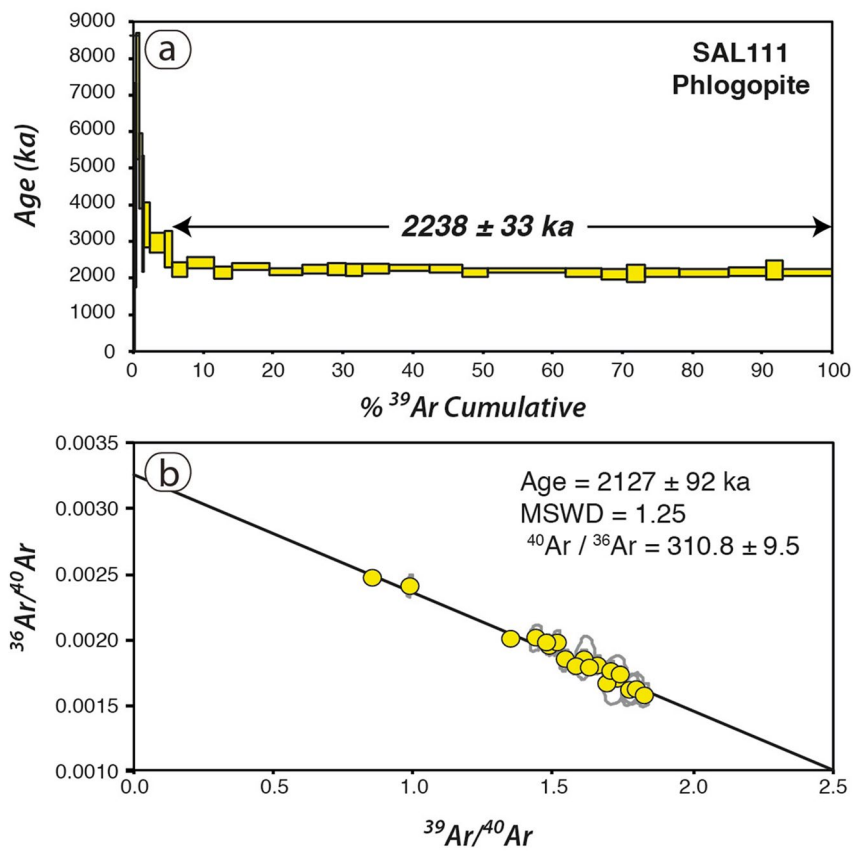

Figure 3. (a) $^{40}Ar/^{39}Ar$ age spectrum and (b) reverse (i.e., $^{36}Ar/^{40}Ar$ vs. $^{39}Ar/^{40}Ar$) isochron diagram of phlogopite crystals in gabbro sample SAL 111.

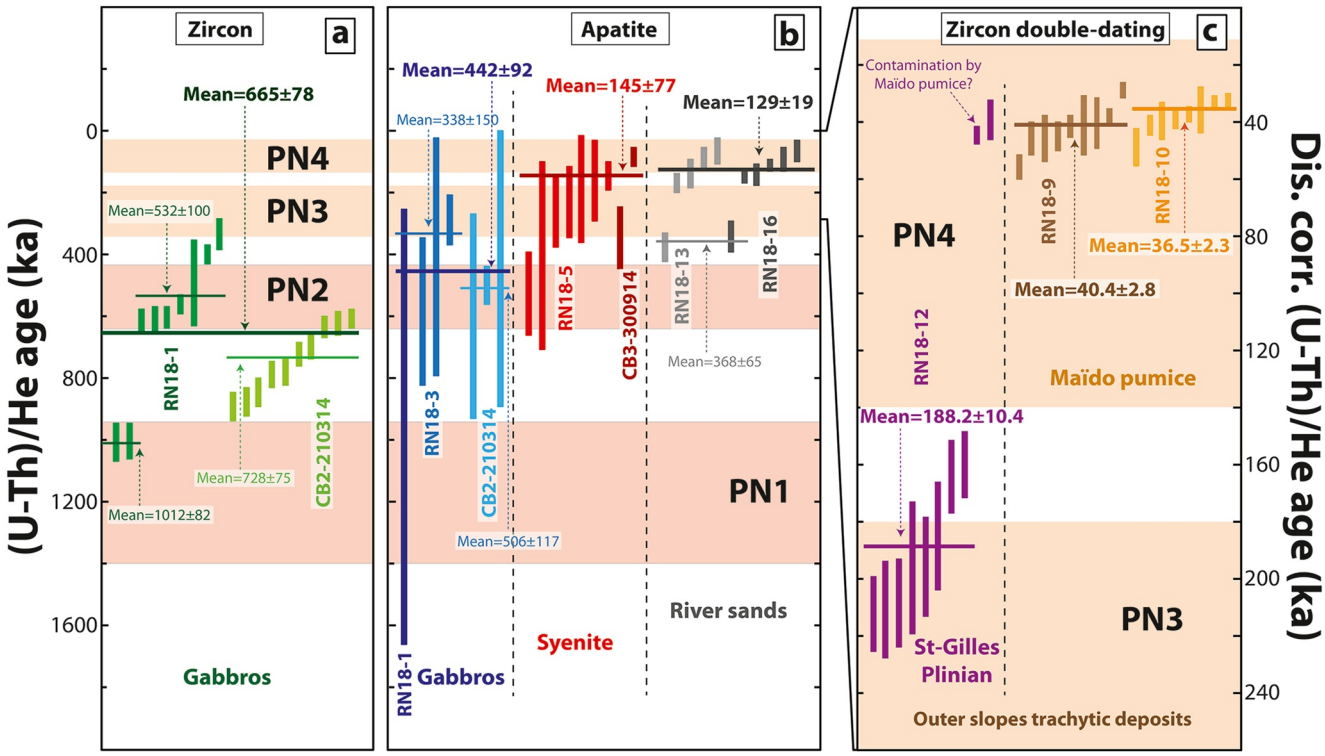

Figure 4. Summary strip plot of (U-Th)/He data displayed as 1σ error bars: (a) and (b) conventional ZHe and AHe data, respectively; (c) ZDD data (i.e., disequilibrium-corrected zircon (U-Th)/He data). Preferred mean values and 2σ uncertainties (in ka) are written in bold letters. Shaded fields correspond to periods of volcanic activity (PN1–PN4) (see Figure 1 for chronostratigraphic chart).

4.1. Gabbros

Two gabbro samples yielded zircon grains, one at Site 4 (RN18-1) and one at Site 3 (CB2-210314). RN18-1 is a layered gabbro, in which 19 analyses from discrete zircon grains yielded a U-Pb concordia intersection age of 2,021 ± 16 ka (uncertainty here and elsewhere is 2σ unless otherwise stated; MSWD = 1.1, Figure 2a). CB2-210314 is a pegmatoid gabbro with blurry contours hosted in the layered gabbro. Thirty-two analyses were made on zircon grains extracted from this pegmatoid gabbro, yielding a U-Pb concordia intersect age of 1,414 ± 8 ka (MSWD = 2.3; Figure 2b).

$^{40}Ar/^{39}Ar$ dating on late magmatic phlogopite crystals separated from sample SAL111 (Site 3), also a layered gabbro, yielded a plateau age of 2,238 ± 33 ka calculated on 21 heating-steps and related to 94.46% of the ^{39}Ar released (Figure 3a). The first heating steps have older ages and higher Ca/K and Cl/K ratios, suggesting that phlogopite is contaminated by a minor amount of weakly bound excess argon. The reverse isochron diagram provided an intercept age of 2,127 ± 92 ka within uncertainty of the plateau age (Figure 3b) and an initial argon ratio of 310.8 ± 9.5 slightly above the reference value of 298.6 (Lee et al., 2006), thus suggesting that a minor amount of excess argon has been also trapped in the phlogopite lattice at the time of its isotopic closure for argon.

(U-Th)/He analyses of nine zircon crystals from sample RN18-1 (Site 4) yielded two age populations (Figure 4), a minor one at 1,012 ± 82 ka (n = 2) and a more prominent one at 532 ± 100 ka (n = 7). Ten zircon crystals from sample CB2-210314 (Site 3) yielded an average ZHe date of 728 ± 75 ka. Apatite crystals were extracted from the two layered gabbro samples at Site 4 (RN18-1 and RN18-3) and from the pegmatoid gabbro at Site 3 (CB2-210314). These apatites, and those from the syenite samples (see Section 4.2), proved challenging to date precisely by (U-Th)/He due to their very low U and Th contents (typical eU of <10 ppm), which in combination with a very young cooling age (typically <500 ka) resulted in extremely imprecise (U-Th)/He dates (total analytical uncertainty often >100%). Therefore, AHe dates need to be interpreted with caution. Four AHe dates from the two layered gabbro samples (merging RN18-1 and RN18-3 data) yielded a mean value of 338 ± 150 ka; three AHe dates from the pegmatoid gabbro (CB2-210314) average at 506 ± 117 ka.

Table 1
Summary of Multitechnique Radiometric Dating Results

Sample	Lat. (°S)	Lon. (°E)	Altitude (m)	Location	Rock description	U/Pb zircon (ka)	$^{40}Ar/^{39}Ar$ phlogopite (ka)	(U-Th)/He zircon (ka)	(U-Th)/He apatite (ka)
Salazie gabbros									
RN18-1	21.05627	55.50046	661	Ilet à vidot, 100 m upstream of bridge (Site 4)	Coarse gabbro with feldspar layers	2,021 ± 16		1,012 ± 82 532 ± 100	442 ± 92 (RN18-1, -3, and CB2-210314 merged)
RN18-3	21.05649	55.50034	662	Ilet à vidot, 100 m upstream of bridge (Site 4)	Layered gabbro				
CB2-210314	21.05726	55.4940	720	Ilet à vidot, exit track in the canyon (Site 3)	Gabbro pegmatite	1,414 ± 8		728 ± 75	
SAL 111	21.057135	55.49489	720	Ilet à vidot, exit track in the canyon (Site 3)	Layered gabbro		2,110 ± 90		
Outer slopes trachytic deposits									
RN18-9	21.07566	55.38360	2,308	Upper Maïdo slopes, Glacière trail	Trachytic pumice	13 ± 17		40.4 ± 2.8	
RN18-10	21.07997	55.35925	1,630	Maïdo, forest roadcut	Trachytic pumice	29 ± 32		36.5 ± 2.3	
RN18-12	21.04232	55.24803	210	Eperon round-about, Saint-Gilles Plinian fallout	Trachytic tephra			188.2 ± 10.4	
Salazie syenite									
RN18-5	21.05749	55.49406	720	Ilet à vidot, exit track in the canyon	Syenite				145 ± 77 (RN18-5 & CB300914 merged
CB3-300914	21.05726	55.49400	720	Ilet à vidot, exit track in the canyon	Syenite				
River sands									
RN18-4	21.05532	55.50072	651	Ilet à vidot below suspended bridge, Salazie	Detrital sand	2,051 ± 26			
RN18-13	21.1144	55.45770	1,100	Bras Rouge river upstream, Cilaos	Detrital sand				368 ± 65 129 ± 19 (RN18-13 & -16 merged)
RN18-16	21.19195	55.44993	340	Bras Rouge river downstream, Cilaos	Detrital sand				

4.2. Syenite Intrusions

Syenite samples yielded apatite but no zircon. The low U and Th contents of these apatites and their young cooling ages result in low-precision AHe dates. Nine apatite grains from two samples of the Salazie syenite laccolith (RN18-5 and CB3-300914, both collected at Site 3), yielded an average of 145 ± 77 ka (Figure 4).

4.3. Trachytic Tephras

Zircon was found in the three tephra samples: RN18-9, RN18-10, and RN18-12. RN18-9 comes from a 1 m-thick pyroclastic density current (PDC) deposit of coarse (up to 10 cm in diameter) trachytic pumice covering the Maïdo upper slopes. U-Th crystallization ages from this sample range from 75.6 +15.9/−13.9 to 29.4 +7.7/−7.2 ka (1σ uncertainties). Ft-corrected (U-Th)/He dates, corrected for disequilibrium, yield a best fit eruption age of 40.4 ± 2.8 ka (Figure 4). RN18-10 also comes from a 2 m-thick PDC level containing coarse trachytic pumice covering a paleo-soil. U-Th crystallization ages (60.3 +14.5/−12.8 ka to 40.6 +11.8/−10.7) for sample RN18-10

fall within the range of U-Th ages of sample RN18-9. Ft-corrected (U-Th)/He dates, that is, corrected for disequilibrium, yield a best fit eruption age of 36.5 ± 2.3 ka. Sample RN18-12 was collected in a 60 cm-thick level of trachytic lapilli ≤0.5 cm in diameter belonging to the Saint-Gilles Plinian deposit. Two distinct age populations were found in this sample, a dominant one (eight analyses) with crystallization ages from >350 to 217 +30.5/−23.8 ka and best fit eruption age of 188.2 ± 10.4 ka, and two analyses with significantly younger U-Th crystallization and (U-Th)/He ages (40.4 +6.8/−6.8 and 83.6 +25.3/−20.5 ka, and 45.5 ± 3.2, and 39.7 ± 7.1 ka, respectively).

4.4. River Sands

Six U-Pb dated zircon crystals from the sand sample of Salazie (RN18-4), collected in the Mât river running through the gabbro at Site 4, yielded a lower intercept on concordia of 2,051 ± 26 ka (MSWD = 0.92; Figure 2c). This age is within uncertainty of the U-Pb age of the layered gabbro at this site (RN18-1) and thus likely derived from this rock unit. Only apatite (no zircon) was found in the two sand samples collected in the cirque of Cilaos. These two samples, collected upstream (RN18-13) and downstream (RN18-16) in the Bras Rouge river, yielded similar AHe dates in the range of ca. 390–70 ka (Figure 4). Combining the two samples results in a bimodal age distribution with two age components of 368 ± 65 ka (n = 2) and 129 ± 19 ka (n = 9).

5. Discussion

5.1. Geo-/Thermochronology of Piton des Neiges Plutonic Complex

In total, four radiometric dating techniques (U-Pb on zircon, $^{40}Ar/^{39}Ar$ on phlogopite, and (U-Th)/He on zircon and apatite) were successfully applied to the plutonic complex cropping out in the cirque of Salazie (Table 1). Adopting a closure temperature concept (Dodson, 1973), these dating techniques can be interpreted to record the timing at which the daughter isotopes cease to diffuse, which occurs at different temperatures depending on the isotopic system, the host mineral, the size of crystals and other fast diffusion pathways. The joint application of these dating techniques on the same rock unit may therefore, potentially, be used to reconstruct its cooling history (Figure 5). The often cited closure temperature of the U-Pb system for >100 µm zircons such as those found in the gabbros is >900°C (Cherniak & Watson, 2001), U and Th and the corresponding disequilibrium system being diffusively even more resistant. This temperature is about the solidus temperature of

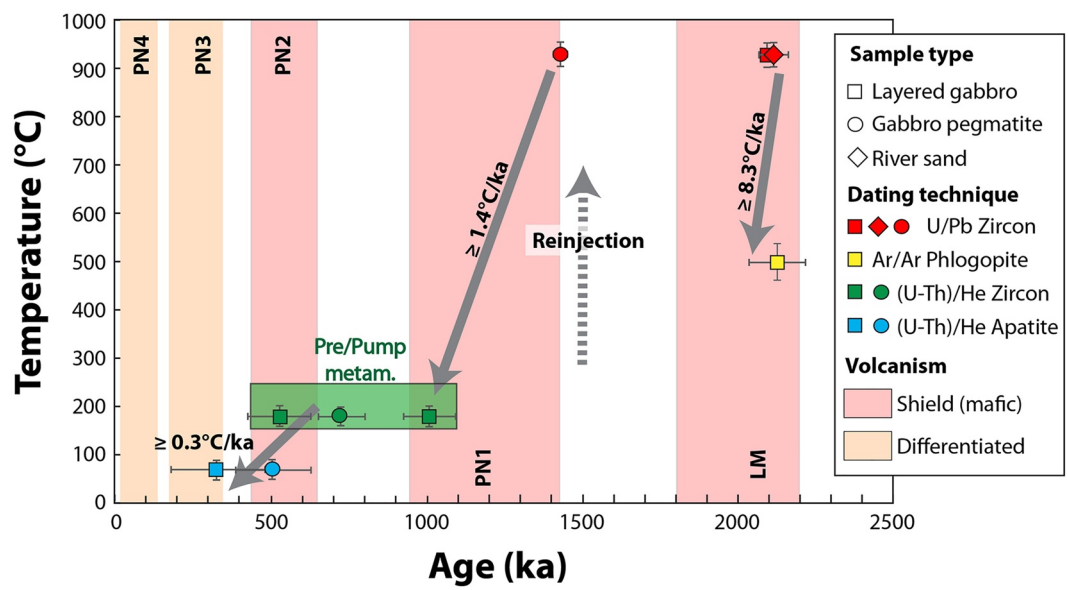

Figure 5. Time-temperature diagram of plutonic rocks from the cirque of Salazie with data from the four dating techniques (U-Pb on zircon, $^{40}Ar/^{39}Ar$ on phlogopite, and (U-Th)/He on zircon and apatite) adopting their closure temperatures as defined in the text. Also represented are known periods of Piton des Neiges volcanism (LM and PN1–PN4) (see Figure 1 for chronostratigraphic chart).

anorthite + clinopyroxene ± phlogopite assemblages such as found in the Salazie gabbros (Famin et al., 2009). Calculated zircon U-Pb ages from the gabbros are therefore interpreted as crystallization ages. All the other dating techniques have much lower closure temperature, and hence are considered as representing cooling ages. Namely, the $^{40}Ar/^{39}Ar$ system in phlogopite closes at ≥500°C in absence of lower-temperature recrystallization (Villa, 2010); the (U-Th)/He system closes at 180°–220°C in zircon and at 60°–80°C in apatite (Farley, 2002; Guenthner et al., 2013).

For the layered gabbro, the isochron age of 2,127 ± 92 ka (SAL 111), taken as the preferred age of the $^{40}Ar/^{39}Ar$ system in phlogopite, falls within uncertainty of the zircon U-Pb ages of 2,021 ± 16 ka (RN18-1) and 2,051 ± 26 ka (RN18-4). These results imply that the layered gabbro cooled down from its solidus to ~500°C in less than a few kyrs and within the first ~200 kyrs of the LM period (Figure 5). In addition, the zircon U-Pb age of 1,414 ± 8 ka obtained for the pegmatoid gabbro, which is younger than the phlogopite $^{40}Ar/^{39}Ar$ age of the layered gabbro, indicates that at least one magmatic reinjection occurred after the emplacement of the layered gabbro, marking the very beginning of the PN1 period.

The rest of the cooling history of the plutonic complex is provided by ZHe and AHe dates (Figure 5). Interpretation of the (U-Th)/He data is, however, not straightforward due to the lack of geological constraints and the limited quality (i.e., low precision) of some data. The absence of correlation between (U-Th)/He dates and eU or crystal size in the samples suggest that neither radiation damage (Shuster et al., 2006) nor crystal size (Farley, 2002) contributed to the observed dispersion of (U-Th)/He dates. Instead, this dispersion may result from a complex thermal history including short-lived reheating events, which could have occurred during intervals beyond the resolution of our dating techniques. Alternatively, the dispersion could stem from imperfection of dated crystals such as undetected microinclusions trapping U, Th, or He, which can result in deviation of (U-Th)/He dates (e.g., Danišík et al., 2017). Older than expected (U-Th)/He dates are, however, difficult to identify if they do not exceed the ages measured by higher-temperature geo-/thermochronometers (e.g., U-Pb). Since we cannot establish with certainty the reason for the observed dispersion, hence, we adopt a simplified approach and interpret our (U-Th)/He dates as cooling ages applying the closure temperature concept (Dodson, 1973). While doing that, we acknowledge that our data may preserve additional complexities.

The ZHe closure temperature of 180°–220°C (Guenthner et al., 2013) corresponds to the temperature range of the lower greenschist or prehnite/pumpellyite facies metamorphism (150°–240°C, Famin et al., 2016). One way of interpreting the data is to consider all the ZHe age populations from each sample separately. In this case, the three ZHe age populations of 1,012 ± 82 ka, 728 ± 75 ka, and 532 ± 100 ka obtained in gabbros confirm that this metamorphic event occurred between the end of the PN1 period and the beginning of PN2 and may also suggest a protracted duration of the metamorphic event in the last ca. 470 kyrs. Given the geographic proximity of all the gabbros (layered and pegmatoid; Figure 1), an alternative way of interpretation is to treat the ZHe data as belonging to the same geological unit that underwent the same low-temperature cooling history. In this latter case, all single grain ZHe dates from gabbros may be merged, yielding an average cooling age of 665 ± 78 ka (MSWD = 15.5) for the ~180°C isotherm, at the beginning of PN2 (Figure 6a). Likewise, AHe dates in gabbros may be interpreted separately for each sample (506 ± 117 ka and 338 ± 150 ka), or jointly by merging all the data (442 ± 92 ka). Both interpretations lead to the same conclusion that the mafic plutonic complex cooled to 60°–80°C from the end of PN2 to the beginning of PN3 (Figure 6a).

5.2. Timing of Syenite Intrusions

Since the syenites are benmoreitic to trachytic in composition, it is tempting to consider those magmas as intrusive equivalents of the tephras exposed on the outer slopes of Piton des Neiges. However, the noteworthy absence of zircon in the syenite intrusions, and its presence in the tephras, is not consistent with this interpretation. AHe dates for the Salazie syenite loosely constrain the cooling of this laccolith through the 60°–80°C temperature range to 145 ± 77 ka, within uncertainty of the average age of the main population of detrital apatites from the Bras Rouge river in Cilaos, at 129 ± 19 ka (Figure 4). Combined together, these results suggest that most of the apatite-rich magmas cooled down at 150–110 ka, which we consider as the likeliest timing for syenite intrusions. This inference is supported by the age of a small benmoreite dyke, parallel to the Cilaos syenite dyke and at a distance of less than 100 m, dated at 156 ± 8 ka by K-Ar on groundmass (sample 57-D in Kluska, 1997). Syenite intrusions would thus be emplaced at the beginning of the PN4 period (Fig. 6a), that is, after the caldera-forming explosive event but before the terminal activity of Piton des Neiges. It should be noted that despite an overlap in

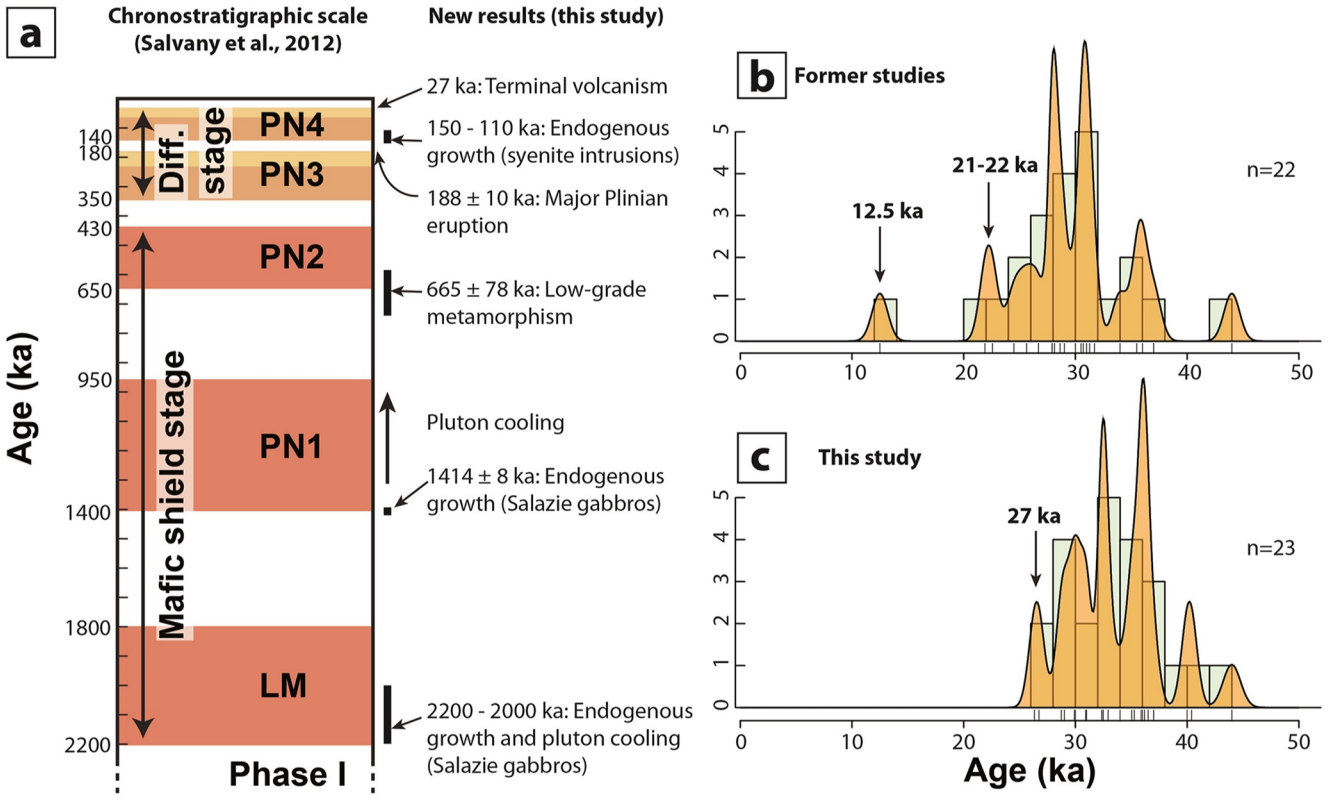

Figure 6. Summary of geological constraints on the history of Piton des Neiges volcano provided by our study. (a) New results reported on the chronostratigraphic chart of Salvany et al. (2012), with colors as in Figure 1. (b) and (c) Temporal distributions (histogram and Kernel density estimation) of radiometric ages on Piton des Neiges for the past 50 ka, before and after our application of ZDD and calibration of ^{14}C ages, respectively.

their respective uncertainties, the timing of cooling of the Salazie syenite laccolith is statistically younger than the AHe dates from the surrounding gabbros (≥338 ± 150 ka), suggesting that the syenitic magmatism was not associated with any heat flux sufficient to thermally reset apatite crystals from the mafic plutonic complex.

5.3. Trachytic Tephras and the Latest Activity of Piton des Neiges

The oldest trachytic tephra found on the western slopes of Piton des Neiges is the Saint-Gilles Plinian deposit (RN18-12), dated at 188.2 ± 10.4 ka (Figure 4). Based on a geochemical comparison, this deposit has been correlated to a marine tephra layer (R6-11) found in an offshore core north-east of Réunion (S17-662) which has been dated at 175 ± 5 ka by calibration on the SPECMAP curve (Fretzdorff et al., 2000). Our ZDD results suggest that the Plinian deposit is in fact slightly older than that, although both ages overlap within uncertainty. Our reappraisal of the Saint-Gilles Plinian deposit age also makes it coeval, within uncertainty, with two major ignimbrite flows filling the cirque of Salazie, at 193 ± 26 ka (sample IM-1 dated by K-Ar on groundmass; Gillot & Nativel, 1982) and 184 ± 10 ka (sample 45-ZB dated by K-Ar on groundmass; Kluska, 1997), both corresponding to the formation of a major caldera. Two other offshore trachytic ash layers better match the timing of the Saint-Gilles Plinian deposit, one at 186 ± 5 ka interpreted as a secondary turbiditic deposit (layer 937 in core MD11-3347 south of Réunion; Lebas, 2012), and the other at ~183 ka interpreted as a true tephra (layer R6-12, core S17-666 north-west of Réunion in Fretzdorff et al., 2000). Both layers could correspond to the offshore record of one of the major caldera-forming explosive episodes that produced the Saint-Gilles Plinian eruption. We note the presence of two significantly younger zircon crystals in RN18-12 with ZHe ages of ~40 ka, which are indistinguishable from the ages of samples RN18-9 and RN18-10 (Figure 4). We interpret these as contaminants deposited by the explosive terminal activity of Piton des Neiges.

The youngest eruption age of trachytic tephra obtained in this study corresponds to the coarse-grained block in the PDC level (RN18-10) dated at 36.5 ± 2.3 ka by ZDD (Figure 4). This age is younger than the eruption age of

RN18-9 at 40.4 ± 2.8 ka, although the uncertainties slightly overlap. This result suggests that the trachytic PDC unit covering the upper western slopes is a composite deposit of several explosive events at the end of the Piton des Neiges lifetime. Two ^{14}C ages in the vicinity of RN18-9 at 33.1 ± 1.0 ka and 46.0 ± 1.1 ka cal BP (samples NY-1000 of Deniel et al., 1992, and 67-AT of Kluska, 1997, respectively, after calibration) confirm this inference.

Importantly, the eruption age of 36.5 ± 2.3 ka from the PDC level RN18-10 is somewhat older than the ^{230}Th-^{238}U age of 12.5 ± 3 ka presumably obtained in the same deposit by Deniel et al. (1992), but consistent, within uncertainty, with the K-Ar age of 37.8 ± 6 ka reported by Kluska (1997). Our result thus confirms, with a considerably improved accuracy, the validity of the K-Ar age, and hence casts doubt on the ^{230}Th-^{238}U age of Deniel et al. (1992), with the consequence that this datum should not be considered as reliable when discussing the last activity of Piton des Neiges.

5.4. An Improved History of Piton des Neiges Volcano

Our multitechnique geochronology provides new constraints on the history of volcanism and extinction of Piton des Neiges that could not be otherwise obtained. Some of these new constraints concern the timing of endogenous growth and cooling relative to extrusive volcanic periods (Figures 5 and 6a). As shown above, the layered Salazie gabbro was emplaced before 2,000 ka, during the first ~200 kyrs of the LM period, and cooled down at a rate ≥8.3°C/ka. Similarly, the pegmatoid gabbro, indicative of a second magmatic intrusion episode, occurred at the very beginning of the PN1 period (1,400 ka) and was cooled down to ≤220°C by the end of it (950 ka), or a cooling rate ≥1.4°C/ka. Our results thus document incremental injection steps during periods of shield-building volcanism, with cooling in-between (Figure 5). The growth of the mafic plutonic complex thus proceeded by successive magma pulses and arrests, rather than by the long-lived activity of a magma reservoir during the whole lifetime of the volcano. Petrological and geochemical observations support this inference (Berthod et al., 2020). This type of progressive endogenous growth is comparable to that of many igneous bodies such as the gabbroic plutonic complex of Fuerteventura in the Canary archipelago (Allibon et al., 2011), and cannot be compared to the emplacement of a single large and chemically zoned reservoir active over million years such as the Skaergaard Intrusion in East Greenland (e.g., McBirney, 1995).

No intrusive body was found to correspond to the PN2 period, yet ZHe dates in gabbros and the low-grade metamorphism imply the presence of a thermal event, and hence of plutonism, ending at the beginning of PN2 (665 ± 78 ka). Likewise, AHe dates in gabbros imply that the plutonic complex was cooled to ≤80°C by the end of PN2, which corresponds to a cooling rate ≥0.3°C/ka. Finally, the inferred age of syenites (150–110 ka) is evidence of intrusive activity and cooling below 80°C in the first ~30 ka of the PN4 period.

ZDD also provides insights into magma storage via the temporal repartition of U-Th crystallization ages (Schmitt, 2011). On one hand, U-Th ages for sample RN18-12 ranging from >350 ka to ca. 190 ka and without a noticeable cluster suggest that prior to the Plinian eruption at 188.2 ± 10.4 ka, zircon crystallized in a long-lived magma reservoir for a protracted period of ≥170 kyrs. On the other hand, indistinguishable U-Th crystallization ages in the 75–36 ka range from samples RN18-9 and RN18-10 suggest that these zircon crystals were formed during a new magmatic cycle lasting for a shorter crystallization period of <40 kyrs. The lack of older U-Th crystallization ages in the two young tephras (RN18-9 and RN18-10) suggest that the Plinian eruption at 188.2 ± 10.4 ka (related to a caldera event) exhaustively depleted the crystal reservoir.

An intriguing point concerns the absence of intrusion ages falling in the PN3 period. Chaput et al. (2017) already noticed a lack of plagioclase-rich dykes or sills typical of PN3 in their systematic study of sheet intrusions at Piton des Neiges. This noteworthy absence is even more puzzling in the perspective of our ZDD data, which show that magmas crystallized beneath Piton des Neiges in the 350–190 ka period. The eruptive center of PN3 magmas being located close to the present-day summit (Gayer et al., 2021), this absence suggests that magmas were stored at greater depth than during the other active periods, and that endogenous growth of the upper edifice was very limited during PN3 in comparison with the large volume of lavas emitted at this stage. The reasons of such a lack of intrusive activity during PN3 remain to be elucidated.

Rejecting Deniel et al. (1992)'s ^{230}Th-^{238}U age of 12.5 ± 3 ka on trachytic tephras forces us to re-evaluate the age of Piton des Neiges terminal volcanism (Figures 6b and 6c). Remaining candidates for the latest volcanic activity are a benmoreite lava flow near the Piton des Neiges summit dated at 29 ± 4 ka by the K-Ar method on groundmass (Kluska, 1997), or a trachytic pumice layer of the Bébour-Bélouve forest with two published

uncalibrated ^{14}C charcoal ages at 21.9 ± 0.7 ka (Delibrias et al., 1986) and 22.6 ± 0.7 ka (Deniel et al., 1992). Using OxCal and the SHCal20 southern hemisphere calibration curve (Bronk Ramsey, 2001; Hogg et al., 2020), these two latter ages become 27.0–25.6 ka and 27.5–26.7 ka cal BP, respectively, and thus fall within uncertainty of the K-Ar age of the Piton des Neiges summit. By providing an intercomparison of different dating methods, our new results combined with published ages allow us to suggest that terminal volcanism of Piton des Neiges should be placed at ca. 27 ka rather than at ca. 12.5 ka as proposed earlier (Figures 6b and 6c). This reappraisal is important for the assessment of volcanic hazards in La Réunion, as it restricts the repartition of volcanic deposits younger than 27 ka to the southeastern half of the island, on the less populated slopes of Piton de la Fournaise.

5.5. Implications of Multiapproach Geochronology for Basaltic Volcanoes

Our multitechnique dating study applied to Réunion has several implications for the understanding of basaltic volcanoes in general, both conceptual and methodological. For instance, a conceptual implication is that plutonic or thermal events in basaltic edifices occur essentially at the beginning of volcanic periods, and that heat dissipates quickly before their end. This suggests that endogenous growth in these islands is most significant at the onset of renewed volcanism, while extrusive growth proceeds during the entire course of activity. Eruptive activity can thus remain surprisingly efficient even though magma storage zones are already cooled below their solidus. Following this line of argument, documented activity of a basaltic volcano does not necessarily imply the existence of a magma storage zone in the edifice, especially if the volcanic activity is long-lived (>200 kyrs). This conclusion matches geophysical evidence on Piton de la Fournaise volcano, active since ∼550 ka, and where volumes of erupted lavas during some paroxysmal eruptions can exceed the volume of magma stored in the edifice prior to the eruption (e.g., Peltier et al., 2008). Magmas may thus rise from crustal or mantle levels to the surface without significant storage in the edifice, perhaps because the already-cooled intrusions increase the density of the edifice, enhancing the buoyancy of the liquids.

Another methodological implication of our study is that care should be taken when interpreting radiometric ages of explosive eruptions in basaltic volcanoes, especially in the case of young (i.e., <40 ka) deposits. Some dating techniques, like ^{230}Th-^{238}U disequilibrium on whole rock and magnetic minerals, might yield erroneous results, while other techniques such as K-Ar on groundmass might be affected by large uncertainties (for instance due to the interaction of pumice with atmospheric argon). Crosschecking with another dating method such as ZDD may provide a more accurate alternative to assess the explosive hazard of basaltic volcanoes, where applying other techniques to young vesiculated rocks devoid of phenocrysts is particularly challenging.

Geochronology on accessory minerals is widely applied to continental settings, because these techniques are well suited to older (≥10 Ma) granitic and metamorphic rocks enriched in both parent and daughter radioactive elements. Few studies, however, have attempted these dating techniques to young intraplate volcanic islands, often discouraged by the challenge of analyzing young mafic magmas, both intrusive and extrusive. Our work shows that applying multiapproach geochronology to young mafic volcanism is not only feasible, but also productive in terms of geological information. Most volcanic islands of the Hawai'i, Canary or Crozet archipelagoes have experienced episodes of plutonism, low-grade metamorphism, and explosive activity, which often constitute limits to our geochronological knowledge of their history. Combined techniques such as zircon U-Pb, phlogopite $^{40}Ar/^{39}Ar$, ZHe, AHe, and ZDD can successfully work together to provide a detailed crystallization-cooling history of these basaltic volcanic islands, offering promising applications to geothermal prospecting and hazard assessment in these islands.

6. Conclusions

Multitechnique geochronology (U-Pb on zircon, $^{40}Ar/^{39}Ar$ on phlogopite, (U-Th)/He on zircon and apatite, and U-Th-Pb and (U-Th)/He on zircon) was employed to place age constraints on some important previously unconstrained geologic events in the history of Piton des Neiges volcano. We show, that the major gabbroic pluton of the volcano grew in at least two stages, 2,200–2,000 ka and 1,414 ± 8 ka, cooling down to near-surface temperatures in-between these stages. A thermal event responsible for the low-grade metamorphism observed in the cirques occurred at ca. 665 ± 78 ka. Syenite intrusions are estimated to have been emplaced at 150–110 ka. These new age constraints show that endogenous growth and thermal events did not occur continuously, but rather developed as short-lived magma pulses restricted to the beginning of volcanic periods, and separated by rapid cooling.

We also provide new ages of trachytic deposits which shed light on the cessation of activity of Piton des Neiges. The major Plinian eruption, whose deposits cover the western slopes of Piton des Neiges, yielded an eruption age of 188.2 ± 10.4 ka, in striking consistency with the age of ignimbrites associated with the formation of a caldera. Furthermore, our results allow us to re-evaluate the age of some recent trachytic pumice deposits to 36.5 ± 2.3 ka, instead of 12.5 ± 3 ka as previously published. Discarding this young age leads us to reconsider published ^{14}C ages of ca. 27 ka after calibration as the lower limit of terminal volcanism at Piton des Neiges, more than twice as old as the previous estimate.

A multitechnique geochronology approach offers a promising solution to reconstruct cooling and eruptive histories in intraplate basaltic volcanic islands, typically complicated by multiple intrusive, metamorphic, or explosive events, occurring over a range of temperatures and timescales of the order of 10's ka. Combining geochronological techniques such as zircon U-Pb, phlogopite $^{40}Ar/^{39}Ar$, (U-Th)/He dating of both zircon and apatite, and U-Th-Pb and (U-Th)/He dating of zircon (zircon double-dating, ZDD) can successfully untangle the chronology of these events, and provide useful information about endogenous versus extrusive magma emplacement, and about explosive hazard in basaltic volcanoes.

Conflict of Interest

The authors declare no conflicts of interest relevant to this study.

Data Availability Statement

Data sets for this research are available in these in-text data citation references: Famin et al. (2022).

Acknowledgments
Martin Danišík was supported by the AuScope NCRIS2 program, Australian Research Council (ARC) Discovery funding scheme (DP160102427), and Curtin Research Fellowship. Martin Danišík thanks I. Dunkl for sharing PepiFLEX software for ICP-MS data reduction, A. Frew and C. May for the assistance with zircon dissolution and solution ICP-MS analysis, respectively. Camille Paquez was supported by the company Austral Energy and by the ANRT CIFRE program (agreement n°2017/1175).

References

Allibon, J., Bussy, F., Lewin, É., & Darbellay, B. (2011). The tectonically controlled emplacement of a vertically sheeted gabbro-pyroxenite intrusion: Feeder-zone of an ocean-island volcano (Fuerteventura, Canary Islands). *Tectonophysics*, *500*(1), 78–97. https://doi.org/10.1016/j.tecto.2010.01.011

Berthod, C., Famin, V., Bascou, J., Michon, L., Ildefonse, B., & Monié, P. (2016). Evidence of sheared sills related to flank destabilization in a basaltic volcano. *Tectonophysics*, *674*, 195–209. https://doi.org/10.1016/j.tecto.2016.02.017

Berthod, C., Michon, L., Famin, V., Welsch, B., Bachèlery, P., & Bascou, J. (2020). Layered gabbros and peridotites from Piton des Neiges volcano, La Réunion Island. *Journal of Volcanology and Geothermal Research*, *405*, 107039. https://doi.org/10.1016/j.jvolgeores.2020.107039

Bronk Ramsey, C. (2001). *Development of the radiocarbon calibration program*. Department of Geosciences, The University of Arizona.

Chaput, M., Famin, V., & Michon, L. (2014). Deformation of basaltic shield volcanoes under cointrusive stress permutations. *Journal of Geophysical Research: Solid Earth*, *119*(1), 274–301. https://doi.org/10.1002/2013JB010623

Chaput, M., Famin, V., & Michon, L. (2017). Sheet intrusions and deformation of Piton des Neiges, and their implication for the volcano-tectonics of La Réunion. *Tectonophysics*, *717*, 531–546. https://doi.org/10.1016/j.tecto.2017.08.039

Cherniak, D. J., & Watson, E. B. (2001). Pb diffusion in zircon. *Chemical Geology*, *172*(1), 5–24. https://doi.org/10.1016/S0009-2541(00)00233-3

Danišík, M., Kuhlemann, J., Dunkl, I., Evans, N. J., Székely, B., & Frisch, W. (2012). Survival of ancient landforms in a collisional setting as revealed by combined fission track and (U-Th)/He thermochronometry: A case study from Corsica (France). *Journal of Geology*, *120*(2), 155–173. https://doi.org/10.1086/663873

Danišík, M., Lowe, D. J., Schmitt, A. K., Friedrichs, B., Hogg, A. G., & Evans, N. J. (2020). Sub-millennial eruptive recurrence in the silicic Mangaone Subgroup tephra sequence, New Zealand, from Bayesian modelling of zircon double-dating and radiocarbon ages. *Quaternary Science Reviews*, *246*, 106517. https://doi.org/10.1016/j.quascirev.2020.106517

Danišík, M., Schmitt, A. K., Stockli, D. F., Lovera, O. M., Dunkl, I., & Evans, N. J. (2017). Application of combined U-Th-disequilibrium/U-Pb and (U-Th)/He zircon dating to tephrochronology. *Quaternary Geochronology*, *40*, 23–32. https://doi.org/10.1016/j.quageo.2016.07.005

Danišík, M., Štěpančíková, P., & Evans, N. J. (2012). Constraining long-term denudation and faulting history in intraplate regions by multisystem thermochronology: An example of the Sudetic Marginal Fault (Bohemian Massif, central Europe). *Tectonics*, *31*(2), TC2003. https://doi.org/10.1029/2011TC003012

Delibrias, G., Guillier, M.-T., & Labeyrie, J. (1986). GIF natural radiocarbon measurements X. *Radiocarbon*, *28*(1), 9–68. https://doi.org/10.1017/s0033822200060008

Deniel, C., Kieffer, G., & Lecointre, J. (1992). New 230Th-238U and 14C age determinations from Piton des Neiges volcano, Reunion–A revised chronology for the Differentiated Series. *Journal of Volcanology and Geothermal Research*, *51*, 253–267. https://doi.org/10.1016/0377-0273(92)90126-x

Dodson, M. H. (1973). Closure temperature in cooling geochronological and petrological systems. *Contributions to Mineralogy and Petrology*, *40*(3), 259–274. https://doi.org/10.1007/BF00373790

Duncan, R. A. (1990). The volanic record of the reunion hotspot. *Proceedings of the Ocean Drilling Program, Scientific Results*, *115*, 3–10.

Famin, V., Berthod, C., Michon, L., Eychenne, J., Brothelande, E., Mahabot, M.-M., & Chaput, M. (2016). Localization of magma injections, hydrothermal alteration, and deformation in a volcanic detachment (Piton des Neiges, La Réunion). *Journal of Geodynamics*, *101*, 155–169. https://doi.org/10.1016/j.jog.2016.05.007

Famin, V., & Michon, L. (2010). Volcano destabilization by magma injections in a detachment. *Geology*, *38*(3), 219–222. https://doi.org/10.1130/G30717.1

Famin, V., Paquez, C., Danišík, M., Gardiner, N. J., Michon, L., Kirkland, L. C., et al. (2022). U-Pb, 40Ar/39Ar, (U-Th)/He, and zircon double-dating geochronology of Intrusive and Explosive Activity on Piton des Neiges Volcano, Réunion Island, Version 1.0. *Interdisciplinary Earth Data Alliance (IEDA)*. https://doi.org/10.26022/IEDA/112216

Famin, V., Welsch, B., Okumura, S., Bachèlery, P., & Nakashima, S. (2009). Three differentiation stages of a single magma at Piton de la Fournaise volcano (Reunion hot spot). *Geochemistry, Geophysics, Geosystems*, *10*(1), Q01007 https://doi.org/10.1029/2008GC002015

Farley, K. A. (2002). (U-Th)/He dating: Techniques, calibrations, and applications. *Reviews in Mineralogy and Geochemistry*, *47*(1), 819–844. https://doi.org/10.2138/rmg.2002.47.18

Farley, K. A., Kohn, B. P., & Pillans, B. (2002). The effects of secular disequilibrium on (U–Th)/He systematics and dating of quaternary volcanic zircon and apatite. *Earth and Planetary Science Letters*, *201*(1), 117–125. https://doi.org/10.1016/S0012-821X(02)00659-3

Fretzdorff, S., Paterne, M., Stoffers, P., & Ivanova, E. (2000). Explosive activity of the Reunion Island volcanoes through the past 260,000 years as recorded in deep-sea sediments. *Bulletin of Volcanology*, *62*, 266–277. https://doi.org/10.1007/s004450000095

Gailler, L.-S., & Lénat, J.-F. (2012). Internal architecture of La Réunion (Indian Ocean) inferred from geophysical data. *Journal of Volcanology and Geothermal Research*, *221–222*, 83–98. https://doi.org/10.1016/j.jvolgeores.2012.01.015

Gayer, E., Michon, L., & Villeneuve, N. (2021). Volcanic island multi-stage construction inferred from a simple geometrical approach: Example of Réunion Island. *Geomorphology*, *392*, 107900. https://doi.org/10.1016/j.geomorph.2021.107900

Gillot, P.-Y., & Nativel, P. (1982). K-Ar chronology of the ultimate activity of Piton des Neiges volcano, Réunion Island, Indian Ocean. *Journal of Volcanology and Geothermal Research*, *13*, 131–146. https://doi.org/10.1016/0377-0273(82)90024-5

Guenthner, W. R., Reiners, P. W., Ketcham, R. A., Nasdala, L., & Giester, G. (2013). Helium diffusion in natural zircon: Radiation damage, anisotropy, and the interpretation of zircon (U-Th)/He thermochronology. *American Journal of Science*, *313*(3), 145–198. https://doi.org/10.2475/03.2013.01

Guillou, H., Carracedo, J. C., Torrado, F. P., & Badiola, E. R. (1996). K-Ar ages and magnetic stratigraphy of a hotspot-induced, fast grown oceanic island: El Hierro, Canary Islands. *Journal of Volcanology and Geothermal Research*, *73*(1), 141–155. https://doi.org/10.1016/0377-0273(96)00021-2

Hogg, A. G., Heaton, T. J., Hua, Q., Palmer, J. G., Turney, C. S. M., & Southon, J. (2020). SHCal20 Southern Hemisphere calibration, 0–55,000 years cal BP. *Radiocarbon*, *62*(4), 759–778. https://doi.org/10.1017/rdc.2020.59

Kluska, J.-M. (1997). *Evolution magmatique et morpho-structurale du Piton des Neiges au cours des derniers 500 000 ans, 246pp*. Université de Paris Sud.

Kurz, M. D., Garcia, M. O., Frey, F. A., & O'Brien, P. A. (1987). Temporal helium isotopic variations within Hawaiian volcanoes: Basalts from Mauna loa and Haleakala. *Geochimica et Cosmochimica Acta*, *51*(11), 2905–2914. https://doi.org/10.1016/0016-7037(87)90366-8

Lebas, E. (2012). *Processus de démantèlement des édifices volcaniques au cours de leur évolution : Application à La Réunion et Montserrat et comparaison avec d'autres édifices* (Vol. 379). Institut de Physique du Globe de Paris.

Lee, J.-Y., Marti, K., Severinghaus, J. P., Kawamura, K., Yoo, H.-S., Lee, J. B., & Kim, J. S. (2006). A redetermination of the isotopic abundances of atmospheric Ar. *Geochimica et Cosmochimica Acta*, *70*(17), 4507–4512. https://doi.org/10.1016/j.gca.2006.06.1563

McBirney, A. R. (1995). Mechanisms of differentiation in the Skaergaard intrusion. *Journal of the Geological Society*, *152*(3), 421–435. https://doi.org/10.1144/gsjgs.152.3.0421

McDougall, I., & Harrison, T. M. (1999). *Geochronology and thermochronology by the 40Ar* (39Ar Method2nd ed., p. 269). Oxford University Press.

McDougall, I. A. X. (1971). The geochronology and evolution of the young volcanic island of Réunion, Indian Ocean. *Geochimica et Cosmochimica Acta*, *35*, 261–288. https://doi.org/10.1016/0016-7037(71)90037-8

Morgan, L. E., Renne, P. R., Taylor, R. E., & WoldeGabriel, G. (2009). Archaeological age constraints from extrusion ages of obsidian: Examples from the Middle Awash, Ethiopia. *Quaternary Geochronology*, *4*(3), 193–203. https://doi.org/10.1016/j.quageo.2009.01.001

Peltier, A., Famin, V., Bachèlery, P., Cayol, V., Fukushima, Y., & Staudacher, T. (2008). Cyclic magma storages and transfers at Piton de La Fournaise volcano (La Réunion hotspot) inferred from deformation and geochemical data. *Earth and Planetary Science Letters*, *270*(3–4). https://doi.org/10.1016/j.epsl.2008.02.042

Quidelleur, X., Gillot, P.-Y., Carlut, J., & Courtillot, V. (1999). Link between excursions and paleointensity inferred from abnormal field directions recorded at La Palma around 600 ka. *Earth and Planetary Science Letters*, *168*(3), 233–242. https://doi.org/10.1016/S0012-821X(99)00061-8

Salvany, T., Lahitte, P., Nativel, P., & Gillot, P. (2012). Geomorphology Geomorphic evolution of the Piton des Neiges volcano (Réunion Island, Indian Ocean): Competition between volcanic construction and erosion since 1.4 Ma. *Geomorphology*, *136*, 132–147. https://doi.org/10.1016/j.geomorph.2011.06.009

Schmitt, A. K. (2011). Uranium series accessory crystal dating of magmatic processes. *Annual Review of Earth and Planetary Sciences*, *39*(1), 321–349. https://doi.org/10.1146/annurev-earth-040610-133330

Shuster, D. L., Flowers, R. M., & Farley, K. A. (2006). The influence of natural radiation damage on helium diffusion kinetics in apatite. *Earth and Planetary Science Letters*, *249*(3), 148–161. https://doi.org/10.1016/j.epsl.2006.07.028

Singer, B. S., Jicha, B. R., Condon, D. J., Macho, A. S., Hoffman, K. A., Dierkhising, J., et al. (2014). Precise ages of the Réunion event and Huckleberry Ridge excursion: Episodic clustering of geomagnetic instabilities and the dynamics of flow within the outer core. *Earth and Planetary Science Letters*, *405*, 25–38. https://doi.org/10.1016/j.epsl.2014.08.011

Spell, T. L., Smith, E. I., Sanford, A., & Zanetti, K. A. (2001). Systematics of xenocrystic contamination: Preservation of discrete feldspar populations at McCullough pass caldera revealed by 40Ar/39Ar dating. *Earth and Planetary Science Letters*, *190*(3), 153–165. https://doi.org/10.1016/S0012-821X(01)00382-X

Stacey, J. S., & Kramers, J. D. (1975). Approximation of terrestrial lead isotope evolution by a two-stage model. *Earth and Planetary Science Letters*, *26*, 207–221. https://doi.org/10.1016/0012-821x(75)90088-6

Villa, I. M. (2010). *Disequilibrium Textures versus Equilibrium Modelling: Geochronology at the Crossroads* (Vol. 332, pp. 1–15). Geological Society Special Publication. https://doi.org/10.1144/SP332.1

References From the Supporting Information

Evans, N. J., Byrne, J. P., Keegan, J. T., & Dotter, L. E. (2005). Determination of uranium and thorium in zircon, apatite, and fluorite: Application to laser (U-Th)/He thermochronology. *Journal of Analytical Chemistry*, *60*(12), 1159–1165. https://doi.org/10.1007/s10809-005-0260-1

Farley, K. A., Wolf, R. A., & Silver, L. T. (1996). The effects of long alpha-stopping distances on (U-Th)/He ages. *Geochimica et Cosmochimica Acta*, *60*(21), 4223–4229. https://doi.org/10.1016/S0016-7037(96)00193-7

Friedrichs, B., Schmitt, A. K., McGee, L., & Turner, S. (2020). U–Th whole rock data and high spatial resolution U–Th disequilibrium and U–Pb zircon ages of Mt. Erciyes and Mt. Hasan Quaternary stratovolcanic complexes (Central Anatolia). *Data in Brief*, *29*, 105113. https://doi.org/10.1016/j.dib.2020.105113

Koppers, A. A. P. (2002). ArArCALC—Software for 40Ar/39Ar age calculations. *Computers & Geosciences*, *28*(5), 605–619. https://doi.org/10.1016/S0098-3004(01)00095-4

Li, X. H., Long, W. G., Li, Q. L., Liu, Y., Zheng, Y. F., Yang, Y. H., & Tao, H. (2010). Penglai zircon megacrysts: A potential new working reference material for microbeam determination of Hf–O isotopes and U–Pb age Pb age. *Geostandards and Geoanalysis Research*, *3434*(22), 117–134.

McDowell, F. W., McIntosh, W. C., & Farley, K. A. (2005). A precise 40Ar–39Ar reference age for the Durango apatite (U–Th)/He and fission-track dating standard. *Chemical Geology*, *214*(3), 249–263. https://doi.org/10.1016/j.chemgeo.2004.10.002

Paces, J. B., & Miller, J. D. (1993). Precise U-Pb ages of Duluth Complex and related mafic intrusions, northeastern Minnesota: Geochronological insights to physical, petrogenetic, paleomagnetic, and tectonomagmatic processes associated with the 1.1 Ga Midcontinent Rift System. *Journal of Geophysical Research*, *98*(B8), 13997–14013. https://doi.org/10.1029/93JB01159

Paton, C., Hellstrom, J., Paul, B., Woodhead, J., & Hergt, J. (2011). Iolite: Freeware for the visualisation and processing of mass spectrometric data. *Journal of Analytical Atomic Spectrometry*, *26*(12), 2508–2518.

Reiners, P. W. (2005). Zircon (U-Th)/He thermochronometry. In P. W. Reiners, & T. A. Ehlers (Eds.), *Thermochronology. Reviews in mineralogy and geochemistry* (Vol. 58, pp. 151–176).

Renne, P. R., Balco, G., Ludwig, K. R., Mundil, R., & Min, K. (2011). Response to the comment by W.H. Schwarz et al. on "Joint determination of 40K decay constants and 40Ar*/40K for the Fish Canyon sanidine standard, and improved accuracy for 40Ar/39Ar geochronology" by P.R. Renne et al. (2010). Geochimica et Cosmochimica Acta, *75*(17), 5097–5100. https://doi.org/10.1016/j.gca.2011.06.021

Schmitt, A. K., Stockli, D. F., Niedermann, S., Lovera, O. M., & Hausback, B. P. (2010). Eruption ages of las tres vírgenes volcano (Baja California): A tale of two helium isotopes. *Quaternary Geochronology*, *5*(5), 503–511. https://doi.org/10.1016/j.quageo.2010.02.004

Schmitz, M. D., & Bowring, S. A. (2001). U-Pb zircon and titanite systematics of the fish canyon tuff: An assessment of high-precision U-Pb geochronology and its application to young volcanic rocks. *Geochimica et Cosmochimica Acta*, *65*(15), 2571–2587. https://doi.org/10.1016/S0016-7037(01)00616-0

Sigmarsson, O., Condomines, M., & Bachèlery, P. (2005). Magma residence time beneath the Piton de la Fournaise Volcano, Reunion Island, from U-series disequilibria. *Earth and Planetary Science Letters*, *234*(1), 223–234.

Tetley, N., McDougall, I., & Heydegger, H. R. (1980). Thermal neutron interferences in the 40Ar/39Ar dating technique. *Journal of Geophysical Research B*, *85*(B12), 7201–7205.

Wiedenbeck, M., Allé, P., Corfu, F., Griffin, W. L., Meier, M., Oberli, F., et al. (1995). Three natural zircon standards for U-Th-Pb, Lu-Hf, trace element and REE analyses. *Geostandards Newsletter*, *19*(1), 1–23. https://doi.org/10.1111/j.1751-908X.1995.tb00147.x